Gallium nitride nanowire electromechanical resonators with piezoresistive readout

Jason M. Gray[a] and Charles T. Rogers
Department of Physics, University of Colorado, Boulder, Colorado 80309

Kris A. Bertness and Norman A. Sanford
National Institute of Standards and Technology, Boulder, Colorado 80305

(Received 2 June 2011; accepted 7 July 2011; published 11 August 2011)

The authors report on the fabrication, piezoresistive readout, and frequency response of doubly clamped *c*-axis gallium nitride nanowire (NW) resonators that show mechanical quality factors exceeding 10 000. The devices are fabricated using a combination of lithographic patterning and dielectrophoresis to suspend NWs across 10 μm gaps. An electrostatic gate induces NW vibration, which is electronically detected via NW piezoresistance. The naturally occurring range of NW diameters results in lowest beam resonances in the range of 9–36 MHz, consistent with a Young's modulus of roughly 300 GPa. Mechanical quality factors, Q, as high as 26 000 under vacuum at 8 K are observed. Selective variation of NW temperature by local joule heating while maintaining cold mechanical clamps demonstrates the dominant role of the polycrystalline metallic end clamps in the room-temperature mechanical dissipation. © *2011 American Vacuum Society*.
[DOI: 10.1116/1.3622326]

I. INTRODUCTION

Nanoscale mechanical resonators are of great interest for high-resolution mass and force sensors, where the small resonator mass and high mechanical quality factor (Q, defined as resonance frequency f_0 over full width at half maximum power) lead to increased sensitivity.[1,2] As-grown *c*-axis gallium nitride (GaN) nanowire (NW) mechanical resonators display high Q's of 10^4–10^5 under vacuum (10^{-5} Pa) and near 300 K, as large or larger than that of zinc oxide,[3] silicon,[4–6] and silicon carbide.[7,8] Due to this high Q and low mass, GaN-NW resonators have been demonstrated as mass sensors with subattogram resolution.[9]

These early demonstrations involved as-grown material with electron microscope-based motion detection and as such were impractical for most device environments. In this paper, we report on the fabrication and performance of doubly clamped *c*-axis GaN-NW resonators, constructed from harvested NWs placed on lithographed structures, with a simple piezoresistive readout appropriate for both fundamental NW studies and sensor applications. These experiments represent significant progress toward practical GaN-NW-based resonator devices.

Briefly, the GaN NWs investigated here are grown, catalyst-free, via gas source molecular beam epitaxy on Si (111) substrates.[10] The NWs have a defect-free, wurtzite crystal structure with their *c* axis along the long axis of the NW. They have a typically hexagonal cross section as seen in Fig. 1(a), with diameters ranging from 100 to 500 nm and lengths up to 20 μm, controllable by growth time.

II. FABRICATION

We fabricate the devices on sapphire substrates, patterned using a combination of photolithography and electron beam lithography. The NW is suspended between electrical contacts (composed of either titanium/aluminum or chrome/gold bilayers totaling 500 nm thickness) with a neighboring electrostatic gate for exciting resonant motion. We position the NWs within the lithographed electrode structure in a process that combines dielectrophoresis with a novel electron beam patterned NW alignment trench, which coats the substrate with resist everywhere except where the NW is to be mounted.

Dielectrophoresis is a process wherein an electric field is used to guide the NW into place, a technique commonly employed in the positioning of nanowires.[11,12] For this process, we immerse a piece of the as-grown GaN-NW substrate in isopropyl alcohol and sonicate it for 5–10 s, dispersing the wires throughout the solution. We then dispense a 10 μl drop of this solution over the lithographic structure. A 10 V peak-to-peak ac signal at 10 kHz is applied to the leads on one side of the wafer with the other side of leads grounded. While the drop evaporates, the NWs tend toward increasing electric field, maximized at the intended bridging point. By adding the alignment trench, we find that we can work with large numbers of NWs, capture only a few in the alignment structure, and remove excess NWs with a short ultrasonic step. NWs captured in the alignment resist structure occur with roughly 30% yield, requiring application of approximately three 10 μl drops to load each device. This represents a factor of 6 increase compared to the approximately 5% yield without the trench. Figure 1(b) shows an atomic force microscope (AFM) image of an NW end mounted on a metallic pad, visible through the alignment resist structure.

Once in place in the alignment structure, the NWs receive a plasma cleaning for 2 min with 50 SCCM (standard cubic

[a]Author to whom correspondence should be addressed; electronic mail: jason.gray@colorado.edu

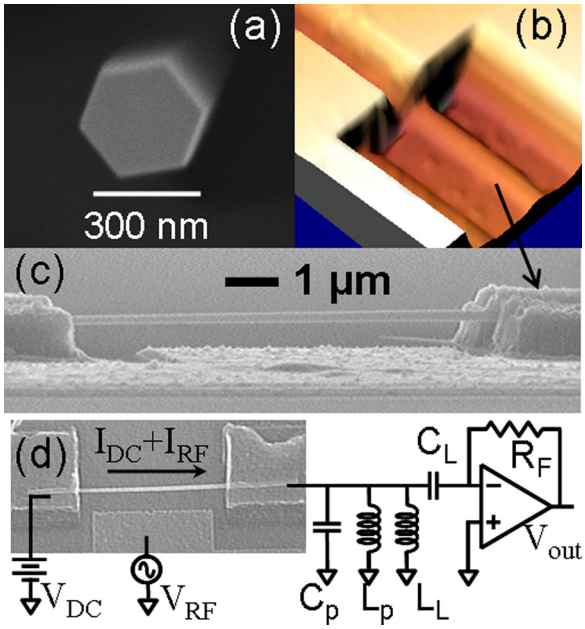

FIG. 1. (Color online) (a) Scanning electron microscope (SEM) image of the hexagonal face of an as-grown NW. (b) AFM image of an NW inside a lithographically defined resist alignment structure after dielectrophoretic mounting. (c) SEM side view image (80° to normal) of the finished device, with Ohmic-contact metal clamping wire and electrostatic gate 1 μm away. (d) Circuit diagram of electronic readout. Direct current voltage (V_{dc}) applied to NW, rf voltage (V_{rf}) applied to gate, generating a dc current and, on resonance, an rf current. Parasitic shorting capacitance (C_p) in cables is canceled at the NW's resonance frequency with inductor L_p. L_L and C_L form an L network to impedance match the NW to the transimpedance amplifier, whose gain is determined by the feedback resistor R_F (~35,000).

centimeter per minute) O_2 at 50 W. We then evaporate the Ohmic-contact metal, consisting of 20 nm of titanium followed by 100 nm of aluminum, using the alignment structure as a mask. The evaporation is done at an angle (30° from normal) to shadow the suspended portion of the wire while still exposing the ends over the pads. With this procedure, no annealing is required to produce approximately Ohmic contacts with NW resistances typically in the range of 100 kΩ–1 MΩ.

To complete the device, we perform another layer of electron beam lithography and metallization for the electrostatic gate. The suspended NWs are robust to this further processing and can survive the additional resist spins, baking, etc. The gate consists of a 20 nm titanium/180 nm aluminum bilayer and is designed to run along the length of the wire, with a typical separation of 1–3 μm. Sweeping an rf voltage on the gate through the NW's resonance then induces vibration due to the capacitive coupling between the gate and NW. Figure 1(c) shows a scanning electron micrograph side view displaying a typical suspended NW resonator.

III. READOUT AND MEASUREMENT

Our electronic readout of NW vibration is based on the piezoresistive properties of GaN.[13] Vibrational strain causes a change in NW resistance; applying a dc voltage to the wire will then induce not only a dc current to flow, but also a

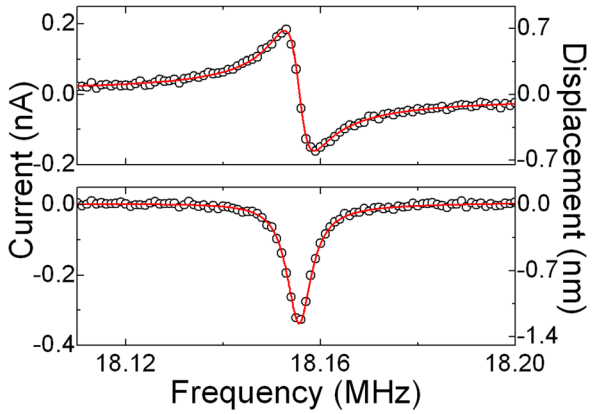

FIG. 2. (Color online) Example of driven NW response under vacuum at room temperature. The left axis shows the rf current through the NW. The right axis displays the calibrated NW deflection based upon the NW thermal Brownian motion as described in the text. Top plot is the in-phase component of the signal measured with rf lock-in, bottom plot is the quadrature phase, with both fitted simultaneously to a complex Lorentzian (solid line). The resonance frequency is 18.15544 ± 0.00002 MHz with a width of 6020 ± 80 Hz, for a mechanical $Q = 3020 \pm 40$.

modulated rf current at the resonance frequency that traces out the Lorentzian resonator response.[14] To verify that the resistance change is predominantly piezoresistive rather than a piezoelectric field effect,[15] we measured the field effect for these NWs and found the resistance change to be much smaller than that caused by strain. We note that a variety of cross-modulation techniques involving rf modulation of the gate and the nanowire bias, with detection at difference or sum frequencies, are possible. In this paper, we concentrate on direct detection at the rf resonance frequency.

The electronic readout configuration can be seen in Fig. 1(d). To first order, all that is required for actuation and detection is an rf voltage on the gate, a dc voltage on the NW, and a current amplifier. Additional circuit elements can be added to increase the signal-to-noise ratio, such as an inductor (L_p) to ground after the NW to compensate for the parasitic capacitance (C_p) in the output cables that shorts a portion of the NW's rf current to ground; L_p in parallel with C_p turns this capacitive short into an effective open circuit at the resonance frequency of the NW. We can also insert an L network (L_L and C_L) to impedance match the high-impedance NW to the low-impedance amplifier; thus further improving the signal-to-noise ratio.[16] The NW's output current feeds into a high-speed, low-noise amplifier with an approximate transimpedance gain of 35 000 V/A. The resulting voltage is then measured by either an rf lock-in or a spectrum analyzer.

Figure 2 shows an example of the lock-in detected current signal upon sweeping a drive voltage on the gate through the mechanical resonance of the NW under vacuum (10^{-5} Pa) at room temperature. We detect both in-phase and out-of-phase components of the response and simultaneously fit a standard complex Lorentzian response function to both components. Resonance frequencies on different devices range from 9 to 36 MHz, equating to a Young's modulus consistent with that of bulk GaN (~300 GPa),[17] with most wires displaying two

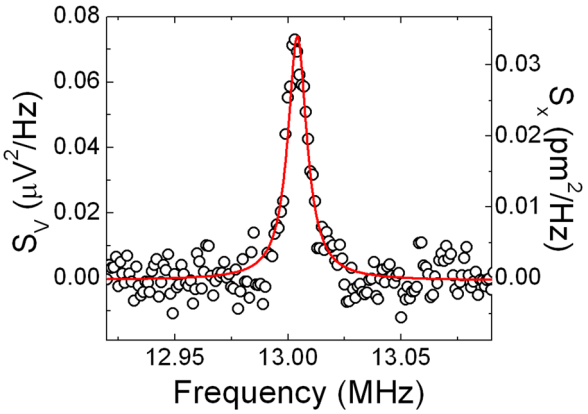

FIG. 3. (Color online) Thermal noise peak of NW (no drive) at 400 K. The axis on the left is the power spectral density of NW (minus amplifier background). The axis on the right is the conversion to picometers through the equipartition theorem. The peak rides on a frequency-independent amplifier background of 5.2×10^{-12} V^2/Hz. The resonance frequency is 13.0042 ± 0.0002 MHz with a width of $10\,200 \pm 600$ Hz, for a mechanical $Q = 1270 \pm 70$.

modes separated by 1–2 MHz (interpreted as the two lowest-order orthogonal modes).

Also shown in Fig. 2 is the associated mechanical deflection scale (right axis) as determined by the observed thermal Brownian motion signal and classical equipartition. Thermal motion occurs because NWs even in vacuum are in contact with a thermal reservoir through the clamps attached to the substrate. Stochastic exchange of thermal energy with the substrate leads to fluctuating drive of the NW vibrational modes and associated stochastic, or Brownian, motion of the nanowire. Our readout scheme is sufficiently sensitive to allow direct observation of this Brownian vibrational noise as in Fig. 3. For this measurement, we apply a dc voltage bias to the NW, reduce the gate drive to zero, and direct the NW current into a spectrum analyzer. A noise peak appears in the power spectral density (PSD) due to this thermal Brownian vibration with a displacement spectral density $S_x(\omega)$ (with units of m^2/Hz) given by[18]

$$S_x(\omega) = \frac{\omega_0}{\left(\omega_0^2 - \omega^2\right)^2 + \left(\omega_0^2/Q\right)^2} \frac{4k_B T}{MQ},$$

where $\omega_0 = 2\pi f_0$, Q is the mechanical quality factor, k_B is the Boltzmann constant (1.38×10^{-23} J/K), T is absolute temperature, and M is the effective resonator mass. Upon integration [and noting that $(1/2\pi)\int_0^\infty S_x(\omega)d\omega =$ mean square displacement $\langle x^2 \rangle$] this simplifies to the classical equipartition theorem, which relates $\langle x^2 \rangle$ to temperature by

$$\frac{1}{2}k\langle x^2 \rangle = \frac{1}{2}k_B T,$$

where $k = M\omega_0^2$ is the effective spring constant of the NW. For one representative device, $k \sim 10$ N/m (estimated with NW mass calculated from physical dimensions as determined by scanning electron microscopy and the known density of GaN, and the measured resonance frequency) and $T \sim 400$ K (elevated due to voltage bias-induced heating), resulting in a total displacement of ~20 pm. Equating that displacement to the integral of the PSD peak then gives the conversion from measured volts to NW central deflection in meters.

Additionally, from the Lorentzian fitting results we can extract mechanical Q, observing values around 1000 for as-fabricated resonators at room temperature. These Q values are lower than the 10^4–10^5 range seen with singly clamped as-grown GaN NWs.[9] This difference is largely attributable to the additional dissipation mechanisms introduced by the doubly clamped devices' fabrication, whereas singly clamped devices are measured as-grown without processing. We proceed to examine these introduced dissipation mechanisms.

IV. REDUCING ENERGY DISSIPATION

One additional source of energy dissipation not present in the as-grown devices is surface contamination. Fabrication leaves the NW coated with organics such as residual electron beam resist. Removing this surface contamination through an O_2 reactive ion etch (RIE) can more than double Q to around 3000 on some devices, though still leaving it below the singly clamped range. Figure 4 shows an example of a single device undergoing successive RIEs, with each further cleaning associated with an increase in Q until an eventual plateau as the contaminants are largely removed.

The next likely source of dissipation is in the polycrystalline metallic clamps on the ends of the NW. To gain insight into this dissipation mechanism, we have investigated the temperature dependence of Q. We find that cooling the substrate to near 8 K at 10^{-4} Pa raises Q to over 10^4 with a highest value to date of 26 000, representing an order of magnitude improvement over the room-temperature measurement. Clearly, cooling freezes out a source of energy dissipation in the system.

To identify the clamps as the source of this dissipation, we selectively increase the NW temperature via local joule heating: Using the NW bias voltage to control heating and NW resistance as an approximate thermometer (calibrated by measuring resistance at low bias as a function of wafer stage temperature and fitting to the roughly linear

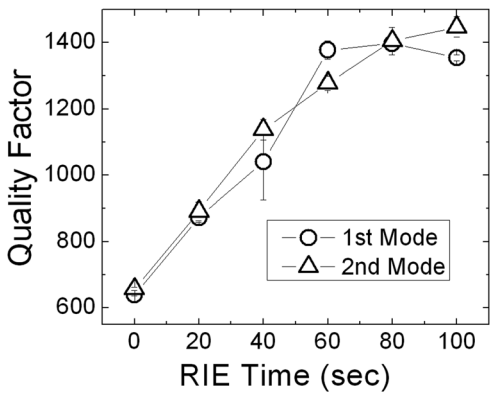

FIG. 4. Successive measurements of quality factor after plasma cleaning with 50 SCCM O_2 at 50 W in an RIE. Circles represent the first mode at 13 MHz. Triangles represent the second mode at 15 MHz.

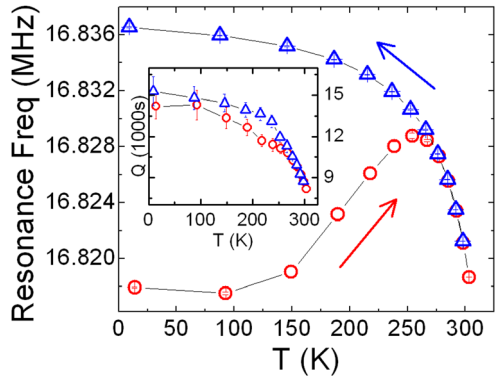

FIG. 5. (Color online) Resonance frequency f_0 vs NW temperature. The temperature scale uses NW resistance as a previously calibrated thermometer. The substrate is at 11 K. Circle data are taken upon initial warming and show an increase in f_0 from evaporating adsorbed species, especially ice. Above ~270 K, f_0 starts decreasing due to the temperature dependence of the Young's modulus of GaN and thermal expansion of the NW held between fixed-spacing clamps. Triangle data are subsequent cooling without additional adsorption, resulting in a higher than initial f_0. Analysis of the frequency shift indicates desorption of total ice mass near 5 fg, or a uniform layer of ice 0.8 nm thick. Inset shows corresponding Q vs NW temperature, reaching ~9000 at room temperature as compared to 900 when the clamps are also at room temperature.

relationship), we can warm the NW to room temperature while the polycrystalline metallic clamps remain cold. Under these circumstances, Q remains high at $\sim 10^4$, implying that the clamps play a large role in the room-temperature energy dissipation.

In Fig. 5 we show an example of this type of study, where we plot NW resonance frequency f_0 and Q versus nominal NW temperature. In this case, the NW was held at 11 K over a period of several hours in modest vacuum of 10^{-2} Pa, allowing a layer of adsorbed species (largely water and nitrogen) to form along its surface. Subsequent data are taken at 10^{-4} Pa to slow further adsorption. Warming the NW with increasing bias causes desorption of this icy layer, appearing in the circle data as an initial increase in f_0 as the wire loses mass. This process continues until approximately 270 K when this layer is largely desorbed, at which point we see a decrease in f_0 associated with the temperature dependence of the Young's modulus[19] of GaN (Ref. 20) and the thermal expansion of the NW between fixed clamps. The triangle data show subsequent cooling behavior as we decrease the NW bias and allow it to return to 11 K. The final value of f_0 is significantly higher than the initial value due to the surface adsorbates not yet having readsorbed along the NW.

The observed behavior of f_0 provides confirmation that the NW temperature is fairly reported by NW resistance. Note then that the measured Q under conditions wherein the NW is warm and clamps are cold remains well above 10^4 over most of the temperature range, and in all cases at least an order of magnitude higher than we find for this device when the entire chip is at 300 K. These results strongly implicate the clamps as major sources of room-temperature dissipation, and suggest that modification of the clamps may enable higher-Q operation of the doubly clamped resonator device at room temperature.

V. CONCLUSION

We have demonstrated the fabrication of doubly clamped GaN-NW mechanical resonators with a piezoresistive readout scheme. This readout is sensitive enough to measure thermal vibration of the NW. Mechanical Q above 2000 at 300 K after plasma cleaning with resonance frequencies around 10 MHz is typical in the devices, while Q above 10^4 is realized by operation with cold mechanical clamps. These relatively high values, comparable to those seen in other materials,[4,8,21] and the simple electronic drive and readout make these devices of immediate utility in high-resolution mass and force sensing applications.

ACKNOWLEDGMENTS

The studies conducted by the authors from the University of Colorado–Boulder are supported by the DARPA Center on Nanoscale Science and Technology for Integrated Micro/Nano-Electromechanical Transducers (iMINT) and the Defense Advanced Research Projects Agency (DARPA) N/MEMS S&T Fundamentals program under Grant No. N66001-10-1-4007 issued by the Space and Naval Warfare Systems Center Pacific (SPAWAR). The authors also acknowledge early funding support from the National Science Foundation (NSF-CMMI) and General Electric (GE).

[1] K. L. Ekinci, Y. T. Yang, and M. L. Roukes, J. Appl. Phys. **95**, 2682 (2004).
[2] C. A. Regal, J. D. Teufel, and K. W. Lehnert, Nat. Phys. **4**, 555 (2008).
[3] R. Zhu, D. Wang, S. Xiang, Z. Zhou, and X. Ye, Nanotechnology **19**, 285712 (2008).
[4] X. L. Feng, R. He, P. Yang, and M. L. Roukes, Nano Lett. **7**, 1953 (2007).
[5] M. Belov, N. J. Quitoriano, S. Sharma, W. K. Hiebert, T. I. Kamins, and S. Evoy, J. Appl. Phys. **103**, 074304 (2008).
[6] J. M. Nichol, E. R. Hemesath, L. J. Lauhon, and R. Budakian, Appl. Phys. Lett. **95**, 123116 (2009).
[7] S. Perisanu, P. Vincent, A. Ayari, M. Choueib, S. T. Purcell, M. Bechelany, and D. Cornu, Appl. Phys. Lett. **90**, 043113 (2007).
[8] X. L. Feng, C. J. White, A. Hajimiri, and M. L. Roukes, Nat. Nanotechnol. **3**, 342 (2008).
[9] S. M. Tanner, J. M. Gray, C. T. Rogers, K. A. Bertness, and N. A. Sanford, Appl. Phys. Lett. **91**, 203117 (2007).
[10] K. A. Bertness, A. Roshko, L. M. Mansfield, T. E. Harvey, and N. A. Sanford, J. Cryst. Growth **310**, 3154 (2008).
[11] P. A. Smith, C. D. Nordquist, T. N. Jackson, T. S. Mayer, B. R. Martin, J. Mbindyo, and T. E. Mallouk, Appl. Phys. Lett. **77**, 1399 (2000).
[12] Y. Liu, J. H. Chung, W. K. Liu, and R. S. Ruoff, J. Phys. Chem. B **110**, 14098 (2006).
[13] A. D. Bykhovski, V. V. Kaminski, M. S. Shur, Q. C. Chen, and M. A. Khan, Appl. Phys. Lett. **68**, 818 (1996).
[14] M. Li, H. X. Tang, and M. L. Roukes, Nat. Nanotechnol. **2**, 114 (2007).
[15] X. Wang, J. Zhou, J. Song, J. Liu, N. Xu, and Z. L. Wang, Nano Lett. **6**, 2768 (2006).
[16] J. B. Hagen, *Radio Frequency Electronics* (Cambridge University Press, Cambridge, UK, 1996), pp. 10–13.
[17] R. Nowak, M. Pessa, M. Suganuma, M. Leszczynski, I. Grzegory, S. Porowski, and F. Yoshida, Appl. Phys. Lett. **75**, 2070 (1999).
[18] A. N. Cleland, *Foundations of Nanomechanics* (Springer, Berlin, 2003).
[19] U. Gysin, S. Rast, P. Ruff, E. Meyer, D. W. Lee, P. Vettiger, and C. Gerber, Phys. Rev. B **69**, 045403 (2004).
[20] Z. Wang, X. Zu, L. Yang, F. Gao, and W. J. Weber, Phys. Rev. B **76**, 045310 (2007).
[21] A. K. Huttel, G. A. Steele, B. Witkamp, M. Poot, L. P. Kouwenhoven, and H.S.J. van der Zant, Nano Lett. **9**, 2547 (2009).